Rayleigh theory of ultrasound scattering applied to liquid-filled contrast nanoparticles

MB Flegg[1], CM Poole[1], AK Whittaker[2], I Keen[2], CM Langton[1]

[1] Faculty of Science & Technology, Queensland University of Technology, Brisbane, Australia

[2] Australian Institute for Bioengineering and Nanotechnology, University of Queensland, Brisbane, Australia

E-mail: christian.langton@qut.edu.au

Abstract. We present a novel modified theory based upon Rayleigh scattering of ultrasound from composite nanoparticles with a liquid core and solid shell. We derive closed form solutions to the scattering cross-section and have applied this model to an ultrasound contrast agent consisting of a liquid-filled core (Perfluorooctyl Bromide, PFOB) encapsulated by a polymer shell (poly-caprolactone, PCL).

Sensitivity analysis was performed to predict the dependence of scattering cross-section upon material and dimensional parameters. A rapid increase in scattering cross-section was achieved by increasing the compressibility of the core, validating the incorporation of high compressibility PFOB; the compressibility of the shell had little impact on the overall scattering cross-section although a more compressible shell is desirable. Changes in the density of the shell and the core result in predicted local minima in scattering cross-section, approximately corresponding to the PFOB-PCL contrast agent considered; hence, incorporation of a lower shell density could potentially significantly improve the scattering cross-section. A 50% reduction in shell thickness relative to external radius increased predicted scattering cross-section by 50%.

Although it has often been considered that the shell has a negative effect on the echogeneity due to its low compressibility, we have shown that it can potentially play an important role in the echogeneity of the contrast agent. The challenge for the future is to identify suitable shell and core materials that meet the predicted characteristics in order to achieve optimal echogenity.

PACS numbers: 43.20.Fn, 43.30.Gv, 87.57.cj

Submitted to: *Phys. Med. Biol.*

1. Introduction

In 1968, Gramiak and Shah observed sonic echoes produced from saline that was injected by a syringe into the lumen of the aortic root. They speculated that the echoes were caused by scattering from microbubbles of gas (Gramiak & Shah 1968, Gramiak et al. 1969). It was proposed that injection of echogenic agents, consisting of microbubbles, could therefore improve the signal to noise ratio (and thus, image contrast) of echocardiograms. Typically, echocardiograms have poor contrast due to similar acoustic impedances amongst soft tissues (Goldberg et al. 2001). Since 1968, there has been a lot of interest in ultrasound contrast agent technology.

The first generation of ultrasound contrast agents (UCAs) consisted of highly compressible microbubbles that were administered by injection. The high compressibility and low density of the microbubbles made them highly echogenic (Riess 2003, Al-Sahhaf et al. 2002, Phillips et al. 1998). However, the early agents were lost within a short period of time because they quickly dissolved into the blood under high ultrasound and arterial pressures (Hoff et al. 2000, Zheng et al. 2009).

The second generation of UCAs were produced in an attempt to increase the lifespan of the agents in vivo whilst not sacrificing the high echogenicity (Hoff et al. 2000, Zheng et al. 2009, Ye 1996, Allen et al. 2001), which are characteristic of the microbubble contrast agents. A range of commercially available agents were produced that consisted of a microbubble protected by a thin layer of albumin or lipid. These agents have had various clinical successes (Lindner 2004). They have been used for real-time evaluation of blood flow and as a safer alternative for molecular imaging than radionuclide imaging (Lindner et al. 2002). Furthermore, they are cost-efficient and widely available (Klibanov 1999), highly echogenic and therefore uses low concentrations (Klibanov 1999). Despite all the advances in microbubble contrast agent technology, there are many issues that oppose the use of encapsulated microbubbles. These include, but are not limited to; isonification destruction (Klibanov 1999, Stride & Saffari 2003, Yeh & Su 2008), phagocytosis (Yanagisawa et al. 2007), induced arrhythmias (Tran et al. 2009) and difficulty of circulation through the capillary system associated with some particularly large bubbles (Liu et al. 2007). Current research being undertaken is dedicated to improving these problems (Klibanov et al. 1997, Leong-Poi et al. 2003, Lindner et al. 2000, Schumann et al. 2002, Villanueva et al. 1998). A lot of this research is focused on shell compositions (Liu et al. 2005), bubble gas (air or heavy) (Liu et al. 2005), bubble size (for resonance) (Hoff et al. 2000, Ye 1996), accelerated thrombolysis (Mizushige et al. 1999) and surface modifications for use in molecular or targeted imaging such as the introduction of ligands on the surface of the bubbles (Klibanov 1999, Klibanov et al. 1997, Lindner et al. 2000, Klibanov 2005) and even the ability to carry therapeutic payloads (Blomley et al. 2001). Shell compositions include; polymer, gelatin, phospholipid, lipid, surfactant, galactose/palmitic acid and albumin (Liu et al. 2005). Gases used range from; air, perfluorocarbon, perfluoropropane, perfluorobutane and sulfur hexafluoride (Liu et al. 2005).

The physical explanation for the exceptional echogeneity of microbubbles is their ability to scatter sound. In 1871, in an effort to explain why the sky appeared as blue and changed to red during a sunset, Lord Rayleigh proposed a mathematical description for the scattering of light by small obstacles (Rayleigh 1871). The same principle applies to sound waves. Most of the research on scattering of sound by objects submersed in fluid (both fluid filled, and gas filled objects) was undertaken in the mid 1900's and was used to describe the scattering of sonar from submerged objects (Hasheminejad & Maleki 2008, Gaunaurd & Werby 1991, Stanton et al. 1998, Strifors & Gaunaurd 1992). Most early attempts to model the scattering from submerged objects used partial wave decomposition (the same approach that was used by Lord Rayleigh in 1871) (Kosobrodov 2002, Gaunaurd et al. 1983, Uberall et al. 1979). The wave components in this approach appear as eigenfunctions of the Helmholtz equation or the wave equation (Ye 1996). One important theory that was applied to gas filled objects was the resonant scattering theory (RST). This theory aims to predict the frequencies of sound that are resonant with a particular object, core or shell (Herzenberg et al. 1964). Manufacturing microbubbles to a specific size resonant with the ultrasound is very important for optimal efficiency of the agent. This is because significant increases in the echo amplitude may be achieved by accurate manufacture of the bubbles to the resonant size. A common approach to modelling the resonant microbubble is the Rayleigh-Plesset equation, and modifications thereof, which describe the oscillations in the bubble radius or volume (Zheng et al. 2009, Frinking & De Jong 1997, Leighton 2007). This approach is specific to gas-filled agents. Furthermore, many of the models that have been proposed for scattering of sound have shown that if an object consists of a shell and core (gas- or liquid-filled), the scatter may be highly affected by the properties of the shell despite being relatively thin compared with the dimension of the object (Hoff et al. 2000, Gaunaurd & Werby 1991, Strifors & Gaunaurd 1992, Kosobrodov 2002, Chen & Ding 1999, Gaunaurd & Werby 1986).

A number of researchers have proposed a "wishlist" for the ideal UCA. Some of these attributes include being; echogenic, nontoxic, intravenously and easily administered, capable of passing through pulmonary, cardiac and capillary circulations, stable for recirculation, able to carry therapeutic payloads, biodegradable and biocompatible, target specific adhesive, able to withstand clinical ultrasound pressures and having poor solubility in water (Klibanov 1999, Pisani et al. 2008b, Marti McCulloch et al. 2000, Goldberg et al. 1994).

Whilst it still remains for technology to deliver all the attributes that a perfect UCA should have, in an attempt to fabricate an ultrasound contrast agent that has some of the aforementioned desirable attributes, a new type of liquid-filled capsule ultrasound contrast agent has been receiving increasing attention (Lanza et al. 1996, Wickline et al. 2002, Layre et al. 2006). Primarily, these nanoparticles have been designed to address key issues such as longevity and stability in the body. One of the biggest disadvantages with using a liquid core as the echogenic material rather than gas is that it is relatively incompressible. This means that its echogeneity is orders of magnitude

weaker than that achieveable using microbubbles since its acoustic properties are not usually very dissimilar to that of the surrounding tissues (Lanza et al. 1996). There are, however, suitable liquids that may be used as ultrasound contrast agent cores documented in the scientific literature. Perfluorooctyl Bromide (PFOB) has poor solubility in water (Lanza et al. 1996) and has a very low speed of sound ($\sim$600m/s) and therefore is highly echogenic submersed in a water (Lanza et al. 1996, Wickline et al. 2002, Andr et al. 1990). In particular cases, more than 20dB signal augmentation is achieved when the PFOB-loaded UCA is bound to abundant molecular epitopes (Marsh et al. 2002a). The liquid capsules are often encapsulated by a polymeric shell such as poly(caprolactone) (PCL) or poly(lactide-co-glycolide) (PLGA). These PFOB-polymer agents are both biodegradable (Reed & Gilding 1981) and biocompatible (Yamaguchi & Anderson 1993). They are also more stable than microbubbles and they can have a range of diameters as low as 70nm which allow for efficient transport throughout the whole vasculature (Pisani et al. 2008b). The advantages that come from nanoparticle use come at the severe cost of echogenicity. It is therefore crucial that nanoparticles that are used as UCAs are improved in echogenicity in order to advance the technology.

PFOB nanocapsules have received a lot of interest for their many advantages that they have over microbubbles in ultrasonography as well as other areas such as magnetic resonance imaging (Pisani et al. 2008b, Andr et al. 1990, Ratner et al. 1988, Krafft et al. 2003). Crucial to realising its potential for clinical use is its significantly inferior echogeneity compared to gas-filled agents. It overcomes this significant disadvantage in a number of different ways. First, the superior stability of the agent means that there is no wastage. Second, attaching ligands to the agent or the use of avidin can cause the agent to adhere to target specific locations or aggregate into larger agglomerates (Lanza et al. 1996, Morawski et al. 2004). Third, PFOB-loaded agents can be manipulated by the acoustic radiation force and therefore be made to adhere to the surface of a target and produce highly concentrated zones (Marsh et al. 2007). Adhesion of the liquid-filled nanoparticle to each other or the wall of a tissue is essential for notably increased echo signals (Lanza et al. 1996). Therefore, in the past, mathematical modelling of PFOB-loaded nanocapsules have been restricted to thin films of PFOB along the surface of a target (Marsh et al. 2002a) and morphological models for fabrication protocols (Pisani et al. 2008a). In molecular imaging, however, individual nanocapsules may be used to bind to molecules. Currently there is no record of a mathematical model for the interaction of individual liquid-loaded nanocapsules with the acoustic waves used in ultrasonography.

In this paper, we present a mathematical analysis of ultrasound Rayleigh scattering applied to liquid-filled polymeric nanocapsules. Since the Rayleigh-Plesset equation is used for gas cores, it cannot be applied to liquid-filled agents. Furthermore, the RST cannot be used in this context; this is because liquid cores are much denser than gas and this means that resonance occurs at larger particle sizes. In fact, liquid-filled agents are usually much smaller ($< 1\mu$m) than typical microbubbles ($\sim 1\mu$m to $\sim 10\mu$m depending on manufacturer) (Dayton & Ferrara 2002, Goldberg et al. 1994).

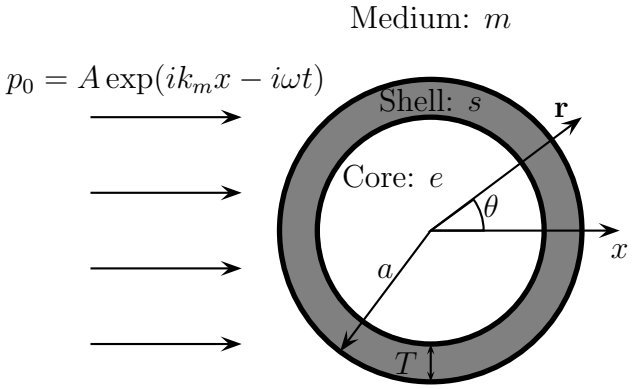

Figure 1. Cross-sectional diagram of ultrasound contrast agent geometry

We therefore use the approach of partial wave decomposition. These partial waves are taken from the eigenfunctions of the Helmholtz equation solved in spherical coordinates. The aim of this analysis is to derive a formula for the scattering cross-section of the capsules dependent on material properties and shell thickness. Particular focus is given to the effect of the shell on the scattering properties of the agent. As the most common modality for nanoparticle UCAs is layered deposition on a target surface it is reasonable to simplify the calculation of echogenicity to the consideration of a thin wall of PFOB (or alternative echogenic material) (Marsh et al. 2002a).We choose to analyse the scattering cross-section of an individual nanoparticle. This is because we consider that the agglomeration of particles on the surface of a target will not act as a homogenous medium. Rather, the particles will each scatter incident waves and the result will be the superposition of the scattered waves. Furthermore, consideration of a homogenous layer of PFOB (nanoparticle core material) will necessarily completely neglect any effect of the nanoparticle shell on the scattering of the wave. As we intend to show, the shell may (if chosen wisely) play an important role in the scattering from each particle and therefore also plays a role in the echogenicity of an agglomeration or layer of such particles. Presenting our analysis of the scattering cross-section in this way, we also leave the results in a form that may be applied to scattering from a single nanoparticle and clouds of nanoparticles. This analysis has never been presented in literature before, however, its potential applications are vast and increasing due to the increase in nanoparticle technology and the widespread nature of Rayleigh scattering in research.

2. Theory

We consider the Rayleigh scattering of sound from a single liquid-filled solid spherical shell. A cross-sectional diagram of the scatterer is provided in Figure 1. The scattering of an incident wave is determined for an angular frequency ω. The pressure wave is

therefore of the form $p_i(\mathbf{r},t) = P_i(\mathbf{r})\exp(-i\omega t)$. The function $P_i(\mathbf{r})$ is the complex wave amplitude and is governed by the Helmholtz equation.

$$\left(\nabla^2 + k_i^2\right) P_i(\mathbf{r}) = 0. \tag{1}$$

In this equation k_i is the wavenumber in the medium of each particular region of the domain represented by the general subscript, i. In this paper, we will use the subscript letter e to represent the liquid core, s to represent the solid shell and m to represent the surrounding medium. We obtain the scattered wave by finding the response of the spherical agent to an incident plane wave $p_0(\mathbf{r},t) = \psi_0(\mathbf{r})\exp(-i\omega t) = A\exp(ik_m x - i\omega t)$. Since the agent is spherically symmetric, we require that the incident wave and the Helmholtz equation be analysed in spherical coordinates (see Figure 1). We write the incident plane wave, therefore, in the following way;

$$\psi_0(\mathbf{r}) = A\exp(ik_m r\cos(\theta)) = A\sum_{h=0}^{\infty}(2h+1)i^h P_h(\cos(\theta))j_h(k_m r), \tag{2}$$

where A is the amplitude of the incident wave and P_n and j_n are well known special functions by the names of the Legendre polynomial of order n and the spherical Bessel function of the first kind of order n, respectively. The incident wave is written in the form of (2) since it is then expressed as a linear combination of eigenfunctions of (1) in spherical coordinates. It is important to notice, here, that (2) is not dependent on the coordinate ϕ. Due to azimuthal symmetry, we therefore also require that the scattered wave does not depend on the azimuthal angle ϕ. (1) holds in all three regions of the domain: the shell, the core and the surrounding medium. We therefore can write the general solution in each part as a linear combination of the eigenfunctions of this equation in spherical coordinates, similar to that of (2). The complex pressure amplitude in any region represented by i is written

$$P_i = \sum_{h=0}^{\infty}\left(a_h j_h(k_i r) + b_h n_h(k_i r)\right) P_h(\cos(\theta)), \tag{3}$$

where a_h and b_h are arbitrary constants that depend on the index h. We therefore write the solutions for the complex pressure amplitude in each of the three regions, external medium, shell and core respectively, as follows

$$P_m = \psi_0 + \sum_{h=0}^{\infty} a_{h;m} h_h(k_m r) P_h(\cos(\theta)); \tag{4a}$$

$$P_s = \sum_{h=0}^{\infty}\left(a_{h;s} j_h(k_s r) + b_{h;s} n_h(k_s r)\right) P_h(\cos(\theta)); \tag{4b}$$

$$P_e = \sum_{h=0}^{\infty} a_{h;e} j_h(k_e r) P_h(\cos(\theta)), \tag{4c}$$

where $n_n(z)$ is called the spherical Bessel function of the second kind of order n and $h_n(z) = j_n(z) + in_n(z)$ is called the spherical Hankel function of the first kind of order n. Notice that in order for the pressure to be finite in the centre of the core $b_{h;e} = 0$. Furthermore, $b_{h;m} = ia_{h;m}$ indicates that any *scattered* wave that travels in the medium must necessarily propagate radially outward from the contrast agent. We now impose physical constraints on the interfaces between the core and the shell and the shell and the external medium. Namely, these conditions are the continuity of pressure across each interface and the continuity of the normal component of particle velocity. Mathematically, these conditions are written in the following way;

$$P_m|_{r=a} = P_s|_{r=a}\,; \tag{5a}$$

$$P_s|_{r=a-T} = P_e|_{r=a-T}\,; \tag{5b}$$

$$\frac{1}{\rho_m}\frac{\partial P_m}{\partial r}\bigg|_{r=a} = \frac{1}{\rho_s}\frac{\partial P_s}{\partial r}\bigg|_{r=a}; \tag{5c}$$

$$\frac{1}{\rho_s}\frac{\partial P_s}{\partial r}\bigg|_{r=a-T} = \frac{1}{\rho_s}\frac{\partial P_e}{\partial e}\bigg|_{r=a-T}, \tag{5d}$$

where ρ_i is the density in the region represented by i. Using both (5b) and (5d) we update (4b),

$$P_s = \sum_{h=0}^{\infty} a_{h;s}\left(j_h(k_s r) + \Gamma_h n_h(k_s r)\right) P_h(\cos(\theta)), \tag{6a}$$

where

$$\Gamma_h = \frac{k_s\rho_e j_h(k_e(a-T))j_h'(k_s(a-T)) - k_e\rho_s j_h(k_s(a-T))j_h'(k_e(a-T))}{k_e\rho_s n_h(k_s(a-T))j_h'(k_e(a-T)) - k_s\rho_e j_h(k_e(a-T))n_h'(k_s(a-T))}, \tag{6b}$$

and the dash notation ($'$) means differentiation with respect to the argument of the function. We find it more convenient to now consider the "effective admittance" of the contrast agent rather than applying conditions (5a) and (5c) directly. The effective admittance for the hth order spherical harmonic is given by β_h and is defined by taking the ratio of the radial component of particle velocity to the pressure (scaled by $\rho_m v_m$ - v_i indicates the speed of sound in the region i) for the hth term in the sum for Ps ($P_{h;s}$) on the shell side of the interface between the shell and the medium. This can be directly calculated from (6) and the definition for radial velocity as shown;

$$u_{r;h} = \frac{1}{i\omega\rho_s}\frac{\partial P_{h;s}}{\partial r}\bigg|_{r=a} = \frac{-\beta_h}{\rho_m v_m}P_{h;s}, \tag{7a}$$

where

$$\beta_h = i\frac{\rho_m v_m}{\rho_s v_s}\frac{j_h'(k_s a) + \Gamma_h n_h'(k_s a)}{j_h(k_s a) + \Gamma_h n_h(k_s a)}. \tag{7b}$$

Defining β_h in this way, allows us to find $a_{h;m}$ more efficiently than direct incorporation of (5a) and (5c) into (4a) and (6). Therefore, we are able to describe the scattered wave in the external media as a result of the incident wave (2). Given the boundary conditions (5a) and (5c), (4a) and (6) and the effective admittance (7b) we can show that the complex scattered pressure wave amplitude is given by

$$\psi = P_m - \psi_0 = \frac{-A}{2}\sum_h (2h+1)i^h(1+R_h)P_h(\cos(\theta))h_h(k_m r), \tag{8a}$$

where R_h, known as the "reflection coefficient", for the case of our encapsulated contrast agent is given by

$$1 + R_h = 2\frac{j_h'(k_m a) + i\beta_h j_h(k_m a)}{h_h'(k_m a) + i\beta_h h_h(k_m a)}. \tag{8b}$$

For Rayleigh scattering, we consider only the first two terms in the sum in (8a). This is because $1 - R_h$ goes to 0 very quickly for $0 < k_m a \ll 1$. Also, we usually only observe the scattered wave many wavelengths from the scattering source. Note, as $k_m r \to \infty$, $i^h h_h(k_m r) \to -(k_m r)^{-1} i\exp(ik_m r)$. Thus (8a) is reduced to

$$\psi = \frac{Ai\exp(ik_m r)}{2k_m r}\left((1+R_0) + 3(1+R_1)\cos(\theta)\right). \tag{9}$$

We are only interested in the scattering angle dependence on the amplitude (rather than the radial dependence) and thus we define the angular dependent scatter to be given by the function

$$\Phi(\theta) = \frac{i}{2k_m}\left((1+R_0) + 3(1+R_1)\cos(\theta)\right) = \gamma_\kappa + \gamma_\rho\cos(\theta), \tag{10}$$

where $\gamma_\kappa = i(1+R_0)/(2k_m)$ and $\gamma_\rho = 3i(1+R_1)/(2k_m)$ will be called the compressibility factor and density factor since each, it can be shown, depends exclusively on the compressibilities (denoted with κ_i in region i) and densities of the materials involved, respectively. The scattering cross-section is calculated from $\Phi(\theta)$. It is defined as the total power scattered (proportional to $|\Phi(\theta)|^2$) divided by the intensity of the incident wave. It is therefore given by the formula

$$\Sigma = 2\pi\int_0^\pi |\Phi(\theta)|^2\sin(\theta)d\theta = 4\pi\left(|\gamma_\kappa|^2 + |\gamma_\rho|^2\right). \tag{11}$$

Furthermore the scattered wave intensity, I_s, at a distance, z, from the scatterer uses the scattering cross-section (Forsberg & Shi 2001).

$$\frac{I_s}{I_0} = \frac{\Sigma}{4\pi z^2}. \tag{12}$$

We can evaluate γ_κ and γ_ρ using (8b), (7b) and (6b), however, this calculation is cumbersome as it involves evaluating spherical Bessel and Hankel functions and their derivatives. Fortunately, since the wavelength of the sound is much larger than the

radius of the scatterer we may make some significant simplifications which are discussed here. Notice that $\gamma_\kappa = \gamma_\kappa(\epsilon)$ and $\gamma_\rho = \gamma_\rho(\epsilon)$, where $\epsilon = T/a$, the ratio of shell thickness to contrast agent radius (see Figure 1). In the thin shell case, $0 < \epsilon \ll 1$, we may write

$$\gamma_\kappa(\epsilon) \approx \gamma_\kappa(0) + \epsilon\gamma'_\kappa(0); \tag{13a}$$

$$\gamma_\rho(\epsilon) \approx \gamma_\rho(0) + \epsilon\gamma'_\rho(0). \tag{13b}$$

$\gamma_\kappa(0)$, $\gamma'_\kappa(0)$, $\gamma_\rho(0)$ and $\gamma'_\rho(0)$ may be calculated from (8b), (7b) and (6b). Taylor series are then taken of all spherical Bessel and Hankel functions to leading order to arrive at our main result (see Appendix 4);

$$\gamma_\kappa \approx \frac{k_m^2 a^3}{3}\left(\frac{\kappa_e - \kappa_m}{\kappa_m} + \frac{3\epsilon}{\kappa_m}(\kappa_s - \kappa_e)\right); \tag{14a}$$

$$\gamma_\rho \approx \frac{k_m^2 a^3}{3}\left(3\frac{\rho_e - \rho_m}{2\rho_e + \rho_m} - 9\epsilon\frac{\rho_m(2\rho_e^2 - \rho_e\rho_s - \rho_s^2)}{\rho_s(2\rho_e + \rho_m)^2}\right). \tag{14b}$$

Notice that when $\epsilon = 0$, we recover the classical Rayleigh compressibility and density factors for a rigid scatterer with no shell (Forsberg & Shi 2001). We can relate the acoustic properties of the composite scatterer to effective properties of a rigid scatterer from classical Rayleigh theory using these formulas. The effective compressibility is given by the volumetric average of the compressibilities within the shell and core and the effective density is given by the nonlinear relationship

$$\rho_{eff} \approx \rho_e + \epsilon\frac{\rho_m(2\rho_e + \rho_s)(\rho_s - \rho_e)}{\rho_s(2\rho_e + \rho_m)}. \tag{15}$$

The usefulness of our derived Rayleigh-Flegg theory for encapsulated nanoparticles is apparent in the prediction of prefered material properties for best contrast. Rayleigh theory is quite explicit in its dependence on particle size. For optimal contrast a larger particle size is desired since $\Sigma \propto a^6$. However, this property is not very interesting because usually the particle size is set by the requirement for agent transport through the cardiopulmonary system. According to (11) and (12), to observe optimal contrast, maximal values of γ_κ and γ_ρ are sought. To achieve this one needs to maximize (14a) and (14b). An important consequence of the compressibility factor and the density factor is that the scattering cross-section is composed of two parts which together produce the scattering cross-section. These factors depend only on the compressibilities and densities, respectively, of the materials involved. In the next section we discuss ways of optimising each part individually by careful choice of material properties. Any change that increases either the compressibility factor or the density factor will result in an increase in the scattering cross-section and ultimately lead to higher echogenicity.

As previously mentioned, when $\epsilon = 0$, we recover the classical Rayleigh compressibility and density factors for a rigid scatterer with no shell (Forsberg & Shi 2001). In the case when $\epsilon = 1$ (shell thickness is equal to the radius of the particle),

we should recover the classical Rayleigh compressibility and density factors for a rigid scatterer with physical properties of the shell (rather than the core). In this situation, (14) cannot be used because these formulae are for thin shells only. Rather one must return to (6b). Using the fact that $a - T \to 0^+$ (note that we can only evaluate the limit. This is because the inner radius becomes 0 and this leads to indeterminate forms of equations such as (6b)) and the expansions in the appendix it is easy to show that $\Gamma_h \to 0$. Thus, (7b) becomes

$$\beta_h \to i\frac{\rho_m v_m}{\rho_s v_s}\frac{j_h'(k_s a)}{j_h(k_s a)}. \tag{16}$$

Substitution into (8b) and then into the definitions $\gamma_\kappa = i(1 + R_0)/(2k_m)$ and $\gamma_\rho = 3i(1 + R_1)/(2k_m)$ leaves

$$\gamma_\kappa \to \frac{k_m^2 a^3}{3}\frac{\kappa_s - \kappa_m}{\kappa_m}; \tag{17}$$

$$\gamma_\rho \to \frac{k_m^2 a^3}{3}\frac{3\rho_s - 3\rho_m}{2\rho_s + \rho_m}, \tag{18}$$

which are the Rayleigh compressibility and density factors for a rigid scatterer with physical properties of the shell. Whilst we do not provide experimental validation of the formulas derived in this paper, they are built from well established mathematical and physical considerations. Furthermore, In both $\epsilon \to 0$ and $\epsilon \to 1$ limits the theory is consistent with classical theory. However, current research is being undertaken to further validate the formulas presented here.

3. Sensitivity analysis

In the following sensitivity analysis, we will assume that the only properties that may be varied are shell and core densities and compressibilities and shell thickness. We will assume that the core has a relatively high compressibility compared to that of the surrounding tissues with approximate water properties; $0 < \kappa_s < \kappa_m < \kappa_e$. Furthermore, we will assume that both ρ_s and ρ_e are $\sim \rho_m$ and we will also limit our discussion to relative shell thicknesses in the region $0 < \epsilon < 0.2$. We will use parameters for a PFOB core, PCL shell and tissue (water) medium and a default shell thickness of $\epsilon = 0.1$. The following parameters are used as default; $\kappa_m = 4.6 \times 10^{-10}\text{ms}^2/\text{kg}$ (calculated from the velocity of sound in water 1480m/s), $\rho_m = 1000\text{kg/m}^3$, $\kappa_e = 1.4 \times 10^{-9}\text{ms}^2/\text{kg} = 3.0\kappa_m$ (calculated from $v_e = 600$m/s (Quaia 2005)), $\rho_e = 1978\text{kg/m}^3 = 1.98\rho_m$ (Marsh et al. 2002b), $\kappa_s = 1.4 \times 10^{-10}\text{ms}^2/\text{kg} = 0.31\kappa_m$ (calculated from $v_s = 2470$m/s (Suh et al. 1995)), $\rho_s = 1145\text{kg/m}^3 = 1.15\rho_m$ (Chouzouri & Xanthos 2007). In each figure, the default PFOB-PCL contrast agent with shell thickness of $\epsilon = 0.1$ is represented by a circle in order to provide orientation to the reader.

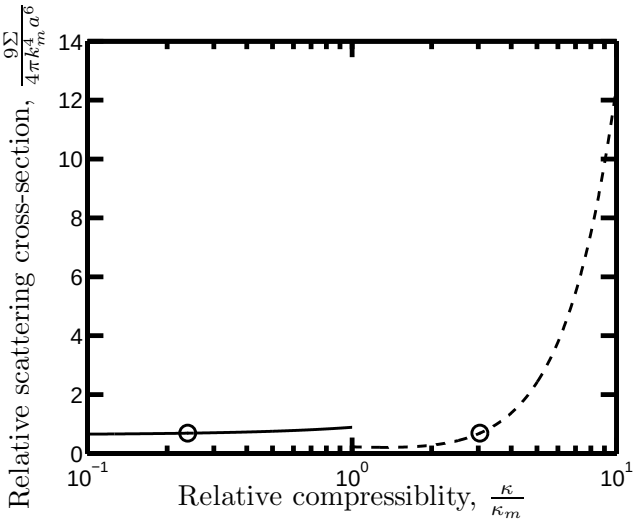

Figure 2. Scattering cross-section versus relative compressibility of both the contrast agent shell (solid) and the contrast agent core (dashed). The circle markers represent the scattering cross-section of PFOB-PCL contrast agents with a shell thickness of $\epsilon = 0.1$.

In Figure 2, the dependence of the scattering cross-section on changes in the compressibility of the shell and the core of the contrast agent according to (11) and (14) are illustrated. The most striking property of this figure is the rapid increase in scattering cross-section that is achievable by increasing the compressibility of the core. This is a well known effect and the reason for the choice of PFOB as the core (indicated by the marker in each figure). PFOB has a high compressibility for a liquid and make it a good choice for the core of the contrast agent. However, significant improvements can be made to liquid-filled contrast agents if more highly compressible, non-toxic and biodegradable liquids can be identified. The compressibility of the shell, as shown in Figure 2 makes little impact on the overall scattering cross-section although a more compressible shell will always be favoured in this respect. The reason for the weak dependence is because the effective compressibility of the contrast agent is given by a volumetric average of the constituent material (see Appendix Appendix A.2 for more details). Since the shell contributes little to the overall volume, it must then weakly contribute to the effective compressibility of the contrast agent.

In Figure 3, the dependence of the scattering cross-section on changes in the density of the shell and the core of the contrast agent according to (14) and (11) are illustrated. The local minima that can be seen in each line represent the situation when $\gamma_\rho = 0$. The local minimum is undesirable (in UCA applications where maximum echogenicity is required) and, according to (14b), occurs when either of the two following conditions are satisfied;

$$\bar{\rho}_e \approx 1 + \epsilon \frac{(1-\bar{\rho}_s)(\bar{\rho}_s+2)}{\bar{\rho}_s}, \tag{19a}$$

$$\bar{\rho}_s \approx \begin{cases} \dfrac{(2\bar{\rho}_e+1)(1-\bar{\rho}_e)}{3\epsilon} - \bar{\rho}_e + \epsilon\dfrac{6\bar{\rho}_e^2}{(2\bar{\rho}_e+1)(1-\bar{\rho}_e)} & 0<\bar{\rho}_e<1 \\ 1+\dfrac{(1-\bar{\rho}_e)(1-3\epsilon)}{3\epsilon} & \bar{\rho}_e \approx 1 \\ \epsilon\dfrac{6\bar{\rho}_e^2}{(2\bar{\rho}_e+1)(\bar{\rho}_e)-1} & \bar{\rho}_e > 1 \end{cases} \tag{19b}$$

where the notation $(\bar{\rho})$ means that the parameter, ρ, has been normalized with respect to the density of the external media ρ_m. It is important to note that there is no strict maximal configuration of material properties but the benefits to be gained by careful choice of material densities are highly interrelated. Away from the local minimum condition (given in (19), the scattering cross-section monotonically increases. Increasing or decreasing the density of the core from the local minimum condition limits to

$$\rho_e \to \infty; \quad \gamma_\rho \to \frac{k_m^2 a^3}{2}\left(1 - 3\epsilon\frac{\rho_m}{\rho_s}\right), \tag{20a}$$

$$\rho_e \to 0; \quad \gamma_\rho \to \frac{k_m^2 a^3}{2}\left(6\epsilon\frac{\rho_s}{\rho_m} - 1\right). \tag{20b}$$

It is desireable to increase the bounds on the density factor according to (20). If one wishes to obtain a high scattering cross-section with a core density above that of condition (19) then according to (20a) one should design the shell to have the smallest, yet practical, density possible and vice versa. Notice also that if a new material for the shell could be used that has a density far *below* that described by (19b) then significant improvements to the scattering cross-section can be made. The reason for this rapid increase is the presence of ρ_s on the denominator of the second term in (14b). Notable, but weaker, increases can be made by further increasing the density from that of PCL. Note that changing the density of a material often means changing its compressibility, so careful selection of the materials is required to create a true increase in scattering cross-section according to (14). The recommendation of the authors to optimize material properties for maximum scatting cross-section is as follows. Primarily, maximize the compressibility of the core. This is because it results in the largest increase in the scattering cross-section with current technology. Secondly, if a number of materials present as candidates for the shell and core (with relatively similar core compressibilities), choose the materials in which maximal density factor is achieved (ones that are furthest from the conditions in (19). The reason for our tendancy to maximize core compressibility as a priority is because, with current material technology, we believe the most gain is to be made in this way. This is already the view portrayed in the literature, however, since echogenicity is one of the main hurdles facing nanoparticle UCAs we recommend keen evaluation of the options using the equations from this manuscript to obtain the best possible scattering cross-section with materials that are available and appropriate. Also, care should be given in the theoretical limit as $\rho_s \to 0$. This is because (14b) would imply an infinite scattering cross-section. However,

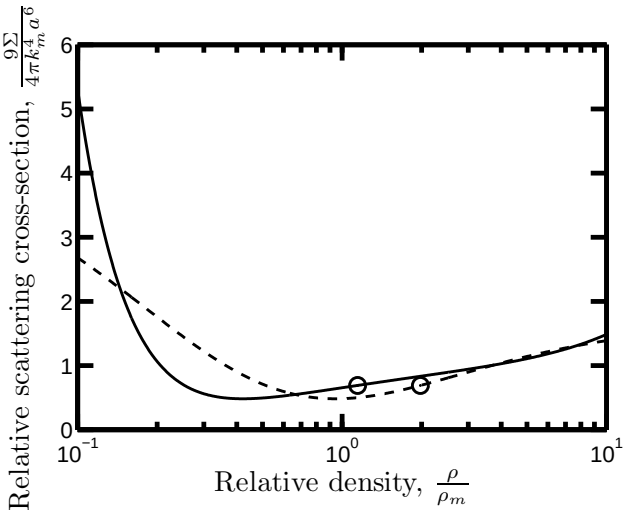

Figure 3. Scattering cross-section versus relative density of both the contrast agent shell (solid) and the contrast agent core (dashed). The circle markers represent the scattering cross-section of PFOB-PCL contrast agents with a shell thickness of $\epsilon = 0.1$.

our assumptions break down in this particular case. $\rho_s \to 0$ implies that there is a layer of vacuum surrounding the core. Such a layer would stop the coupling of sound into the core. However, this contradicts our assumptions. This means that rather than $\gamma_\rho \to \infty$ for $\rho_s \to 0$, the practical limit is, in fact, $\gamma_\rho \to -a$. This can be shown by finding the limit of the exact form of γ_ρ for $\rho_s \to 0$ and $\rho_e \to 0$.

Finally, it is important to critically analyse the geometry of the contrast agent. Aside from the size of the agent, control over the shell thickness is also possible. In Figure 4 the dependence of the scattering cross-section on changes in the shell thickness of the contrast agent according to (14) and (11) are illustrated. The most noteworthy property of this figure is that 'thinner is better'. This is because for PFOB-PCL contrast agents the second term in both (14a) and (14b) reduce the size of γ_κ and γ_ρ, ultimately this means that if we can reduce the relative thickness of the shell, ϵ, then both γ_κ and γ_ρ will increase and therefore the scattering cross-section would also increase according to (11). However, if the density of the shell was such that it was below the condition given in (19b) then the second term in (14b) would be positive and thus one would expect a local maximum in scattering cross-section to occur when the increase in the scattering cross-section due to the second term in (14b) balances the decrease in the scattering cross-section due to the second term in (14a). Advancement in contrast agent materials may also be achieved, therefore, by consideration of the thickness of the shell. For example, if one cannot find a suitable material for the shell which has a very large or very low density then it may be better to choose a material with lower compressibility and more unfavourable density if it can be manufactured to a more stable, thinner, shell. Notice that in Figure 4, increases in scattering cross-section of about 50% can be made by halving the thickness of the shell.

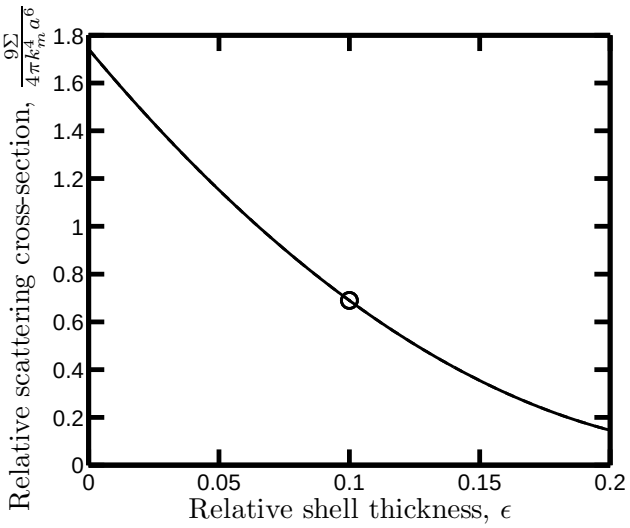

Figure 4. Scattering cross-section versus relative shell thickness for PFOB-PCL contrast agents. The circle marker represents the scattering cross-section of contrast agents with a shell thickness of $\epsilon = 0.1$ for comparison with Figures 2 and 3.

4. Conclusions

In this paper we have presented a theory for Rayleigh scattering from composite nanoparticles consisting of a spherical non-gaseous core coated in a thin solid shell. Such particles can and have already been used as ultrasound contrast agents. This manuscript contains purely theoretical formulae of the scattering cross-section of the UCA nanoparticles according to morphology (size and shell thickness) and material properties. The model assumes that particles have a particular size, are perfectly symmetric and have no acoustic attenuation. This limits the prediction of quantitative experimental results, however, still provides valuable insight into the mechanisms by which sound is scattered from the particles and therefore is a useful tool in evaluation of scattering efficacy of a composite nanoparticle. In our sensitivity analysis we have discussed possible ways of improving the contrast agent's echogeneity based on the outlined theory. These improvements include modifying such material and manufacturing parameters such as core and shell compressibilities and densities and the shell thickness. Whereas it has often been considered that the shell has a negative effect on the echogeneity because of its often low compressibility, we have shown that the shell density can potentially play an important role in the echogeneity of the agent if suitable materials can be found with the desired properties.

Acknowledgments

The research of Dr. MB Flegg is supported by Queensland Cancer Physics Collaborative.

Appendix

Appendix A.1. Derivation of (14)

Consider the definitions $\gamma_\kappa = i(1+R_0)/(2k_m)$ and $\gamma_\rho = 3i(1+R_1)/(2k_m)$. Using (8b), these factors become;

$$\gamma_\kappa(\epsilon) = \frac{ij_0'(k_m a) - \beta_0(\epsilon) j_0(k_m a)}{k_m(h_0'(k_m a) + i\beta_0(\epsilon) h_0(k_m a))}, \tag{A.1a}$$

$$\gamma_\rho(\epsilon) = \frac{3\left(ij_1'(k_m a) - \beta_1(\epsilon) j_1(k_m a)\right)}{k_m(h_1'(k_m a) + i\beta_1(\epsilon) h_1(k_m a))}, \tag{A.1b}$$

where the dependence on ϵ is written explicitly. According to (7b)

$$\beta_h(\epsilon) = i\frac{\rho_m v_m}{\rho_s v_s}\frac{j_h'(k_s a) + \Gamma_h(\epsilon) n_h'(k_s a)}{j_h(k_s a) + \Gamma_h(\epsilon) n_h(k_s a)}, \tag{A.2}$$

where (6b) gives us

$$\Gamma_h(\epsilon) = \frac{k_s\rho_e j_h(k_e a(1-\epsilon)) j_h'(k_s a(1-\epsilon)) - k_e\rho_s j_h(k_s a(1-\epsilon)) j_h'(k_e a(1-\epsilon))}{k_e\rho_s n_h(k_s a(1-\epsilon)) j_h'(k_e a(1-\epsilon)) - k_s\rho_e j_h(k_e a(1-\epsilon)) n_h'(k_s a(1-\epsilon))}. \tag{A.3}$$

Our first order perturbation expansion for γ_κ and γ_ρ (note (13)) are then written

$$\gamma_\kappa(\epsilon) = \gamma_\kappa(0) + \epsilon\left[\frac{\partial\gamma_\kappa}{\partial\beta_0}\frac{\partial\beta_0}{\partial\Gamma_0}\frac{\partial\Gamma_0}{\partial\epsilon}\right]_{\epsilon=0}; \tag{A.4a}$$

$$\gamma_\rho(\epsilon) = \gamma_\rho(0) + \epsilon\left[\frac{\partial\gamma_\rho}{\partial\beta_1}\frac{\partial\beta_1}{\partial\Gamma_1}\frac{\partial\Gamma_1}{\partial\epsilon}\right]_{\epsilon=0}. \tag{A.4b}$$

These derivatives are easily calculated from (A.1), (A.2) and (A.3). Notice that the quantity $k_i a \ll 1$ for each region and therefore, since it is the argument of all spherical Bessel and Hankel functions (and derivatives thereof), first order approximations are used for each of these terms. These approximations are well known but are displayed below for completeness;

$$j_0(k_i a) \to 1; \quad j_0'(k_i a) \to \frac{-k_i a}{3}; \quad j_0''(k_i a) \to \frac{-1}{3}; \tag{A.5a}$$

$$n_0(k_i a) \to \frac{-1}{k_i a}; \quad n_0'(k_i a) \to \frac{1}{(k_i a)^2}; \quad n_0''(k_i a) \to \frac{-2}{(k_i a)^3}; \tag{A.5b}$$

$$h_0(k_i a) \to \frac{-i}{k_i a}; \quad h_0'(k_i a) \to \frac{i}{(k_i a)^2}; \tag{A.5c}$$

$$j_1(k_i a) \to \frac{k_i a}{3}; \quad j_1'(k_i a) \to \frac{1}{3}; \quad j_1''(k_i a) \to \frac{-k_i a}{9}; \tag{A.5d}$$

$$n_1(k_i a) \to \frac{-1}{(k_i a)^2}; \quad n_1'(k_i a) \to \frac{2}{(k_i a)^3}; \quad n_1''(k_i a) \to \frac{-6}{(k_i a)^4}; \tag{A.5e}$$

$$h_1(k_i a) \to \frac{-i}{(k_i a)^2}; \quad h_1'(k_i a) \to \frac{2i}{(k_i a)^3}; \tag{A.5f}$$

Written to lowest order in a, (A.4), using (A.5) and noting that $\kappa = 1/(v^2\rho)$, become (14).

Appendix A.2. Compressibility factor for arbitrary shell thickness

We wish to show that the compressibility factor for the composite nanoparticle can be calculated using the classical form for this factor where the particle compressibility is replaced by the volumetric average of the particle compressibilities (the effective compressibility of the particle is given by an average of the compressibilities of the shell and the core weighted by their respective volumes). Let us try to evaluate Γ_0 from (6b). Using (A.5) we can see that to leading order in a

$$\Gamma_0 = \frac{k_s a^3 (1-\epsilon)^3 (k_s^2 \rho_e - k_e^2 \rho_s)}{3\rho_e} + o(a^3), \tag{A.6}$$

where o is the little-o Landau symbol. Therefore (7b) becomes

$$\beta_0 = -\frac{i\rho_m v_m a}{3\rho_s \rho_e k_s v_s} \left(k_s^2 \rho_e + (k_e^2 \rho_s - k_s^2 \rho_e)(1-\epsilon)^3 \right) + o(a). \tag{A.7}$$

Substitution of β_0 into (8b) for $1 + R_0$ and the knowledge that $k = \omega/v$ and $\kappa = 1/(v^2\rho)$ leads to our result

$$\gamma_\kappa = i(1+R_0)/(2k_m) = \frac{k_m^2 a^3}{3} \frac{\kappa_{\text{effective}} - \kappa_m}{\kappa_m} + o(a^3), \tag{A.8}$$

where

$$\kappa_{\text{effective}} = \left(1 - (1-\epsilon)^3\right) \kappa_s + (1-\epsilon)^3 \kappa_e = \frac{\text{vol}_s \kappa_s + \text{vol}_e \kappa_e}{\text{vol}_s + \text{vol}_e}, \tag{A.9}$$

and vol_s and vol_e are the volumes of the shell and core of the nanoparticle respectively. (14a) is thus the linear perturbation expansion of (A.9) in the case of small ϵ.

References

Al-Sahhaf T, Suttar Ahmed A & Elkamel A 2002 *Petroleum science and technology* **20**(7,8), 773–788.

Allen J S, Kruse D E & Ferrara K W 2001 *IEEE Transactions on Ultrasonics, Ferroelectrics and Frequency Control* **48**(2), 409–418.

Andr M, Nelson T & Mattrey R 1990 *Investigative Radiology* **25**(9), 983.

Blomley M J K, Cooke J C, Unger E C, Monaghan M J & Cosgrove D O 2001 *British Medical Journal* **322**(7296), 1222.

Chen W Q & Ding H J 1999 *The Journal of the Acoustical Society of America* **105**, 174.

Chouzouri G & Xanthos M 2007 *Acta Biomaterialia* **3**, 745–756.

Dayton P A & Ferrara K W 2002 *Journal of Magnetic Resonance Imaging* **16**(4), 362.

Forsberg F & Shi W T 2001 *in* 'Ultrasound contrast agents: Basic principles and clinical applications' Martin Dunitz Ltd London.

Frinking P J A & De Jong N 1997 Vol. 2. 1997 IEEE Ultrasonics Symposium, 1997. Proceedings.

Gaunaurd G C, Tanglis E, berall H & Brill D 1983 *Il Nuovo Cimento B (1971-1996)* **76**(2), 153–175.
Gaunaurd G C & Werby M F 1986 *International journal of solids and structures* **22**(10), 1149–1159.
Gaunaurd G C & Werby M F 1991 *The Journal of the Acoustical Society of America* **90**, 2536.
Goldberg B B, Liu J B & Forsberg F 1994 *Ultrasound in medicine & biology* **20**(4), 319.
Goldberg B B, Raichlen J S & Forsberg F 2001 *Ultrasound contrast agents: basic principles and clinical applications* 2nd edn Martin Dunitz London.
Gramiak R & Shah P M 1968 *Investigative Radiology* **3**(5), 356–366.
Gramiak R, Shah P M & Kramer D H 1969 *Radiology* **92**(5), 939–948.
Hasheminejad S M & Maleki M 2008 *Acoustical Physics* **54**(2), 168–179.
Herzenberg A, Kwok K L & Mandl F 1964 *Proceedings of the Physical Society* **84**, 477–497.
Hoff L, Sontum P C & Hovem J M 2000 *The Journal of the Acoustical Society of America* **107**, 2272.
Klibanov A L 1999 *Advanced drug delivery reviews* **37**, 139–157.
Klibanov A L 2005 *Bioconjugate chemistry* **16**(1), 9–17.
Klibanov A L, Hughes M S, Marsh J N, Hall C S, Miller J G, Wible J H & Brandenburger G H 1997 *Acta radiologica. Supplementum* **412**, 113.
Kosobrodov R A 2002 *Acoustical Physics* **48**(3), 309–320.
Krafft M P, Chittofrati A & Riess J G 2003 *Current Opinion in Colloid & Interface Science* **8**(3), 251–258.
Lanza G M, Wallace K D, Scott M J, Cacheris W P, Abendschein D R, Christy D H, Sharkey A M, Miller J G, Gaffney P J & Wickline S A 1996 *Circulation* **94**(12), 3334.
Layre A, Couvreur P, Chacun H, Richard J, Passirani C, Requier D, Benoit J P & Gref R 2006 *Journal of Controlled Release* **111**(3), 271–280.
Leighton T G 2007. ISVR Technical Report:*Derivation of the Rayleigh-Plesset equation in terms of volume* No **308**
Leong-Poi H, Christiansen J, Klibanov A L, Kaul S & Lindner J R 2003 *Circulation* **107**(3), 455.
Lindner J, Klibanov A & Ley K 2002 *in* V Muzykantov & V Torchilin, eds, 'Biomedical aspects of drug targeting' Kluwer Boston pp. 149–172.
Lindner J R 2004 *Nature Reviews Drug Discovery* **3**(6), 527–533.
Lindner J R, Song J, Xu F, Klibanov A L, Singbartl K, Ley K & Kaul S 2000 *Circulation* **102**(22), 2745.
Liu J B, Wansaicheong G, Merton D A, Forsberg F & Goldberg B B 2005 *Journal of Medical Ultrasound* **13**(3), 109–126.
Liu J, Li J, Rosol T J, Pan X & Voorhees J L 2007 *Physics in medicine and biology* **52**(16), 4739–4748.
Marsh J N, Hall C S, Scott M J, Fuhrhop R W, Gaffney P J, Wickline S A & Lanza G M 2002 *IEEE Transactions on Ultrasonics, Ferroelectrics and Frequency Control* **49**(1), 29–38.
Marsh J N, Hall C S, Wickline S A & Lanza G M 2002 *Journal of the Acoustical Society of America* **112**(6), 2858–2862.
Marsh J N, Partlow K C, Abendschein D R, Scott M J, Lanza G M & Wickline S A 2007 *Ultrasound in medicine & biology* **33**(6), 950–958.
Marti McCulloch R, Cris Gresser R, Sally Moos R, Jill Odabashian R, Susan Jasper B S N, Jim Bednarz R, Pam Burgess R, Dennis Carney R, Vickie Moore R & Eric Sisk R 2000 *J Am Soc Echocardiogr* **13**, 959–67.
Mizushige K, Kondo I, Ohmori K, Hirao K & Matsuo H 1999 *Ultrasound in medicine & biology* **25**(9), 1431–1437.
Morawski A M, Winter P M, Crowder K C, Caruthers S D, Fuhrhop R W, Scott M J, Robertson J D, Abendschein D R, Lanza G M & Wickline S A 2004 *Magnetic Resonance in Medicine* **51**(3), 480–486.
Phillips D, Chen X, Baggs R, Rubens D, Violante M & Parker K J 1998 *Ultrasonics* **36**, 883–892.
Pisani E, Fattal E, Paris J, Ringard C, Rosilio V & Tsapis N 2008 *Journal of Colloid And Interface Science* **326**(1), 66–71.
Pisani E, Tsapis N, Galaz B, Santin M, Berti R, Taulier N, Kurtisovski E, Lucidarme O, Ourevitch M & Doan B T 2008 *Adv Funct Mater* **18**(19), 29632971.

Quaia E 2005 *Contrast media in ultrasonography: basic principles and clinical applications* Springer, Berlin Heidelberg New York.

Ratner A V, Muller H H, Bradley-Simpson B, Johnson D E, Hurd R E, Sotak C & Young S W 1988 *Investigative Radiology* **23**(5), 361.

Rayleigh L 1871 *Philosophical Magazine* **41**, 447–454.

Reed A M & Gilding D K 1981 *Polymer* **22**, 494–8.

Riess J G 2003 *Current Opinion in Colloids and Interface Science* **8**(3), 259–266.

Schumann P A, Christiansen J P, Quigley R M, McCreery T P, Sweitzer R H, Unger E C, Lindner J R & Matsunaga T O 2002 *Investigative Radiology* **37**(11), 587.

Stanton T K, Chu D & Wiebe P H 1998 *The Journal of the Acoustical Society of America* **103**, 236.

Stride E & Saffari N 2003 *Ultrasound in Medicine & biology* **29**(4), 563–573.

Strifors H C & Gaunaurd G C 1992 *Ultrasonics* **30**(2), 107–112.

Suh K S, Lee H J, Lee D S & Kang C G 1995 *IEEE Transactions on Dielectrics and Electrical Insulation* **2**(3), 460–466.

Tran T A, Le Guennec J Y, Babuty D, Bougnoux P, Tranquart F & Bouakaz A 2009 *Ultrasound in Medicine & Biology* **35**(6), 1050–1056.

Uberall H, George J, Farhan A R, Mezzorani G, Nagl A, Sage K A & Murphy J D 1979 *The Journal of the Acoustical Society of America* **66**, 1161.

Villanueva F S, Jankowski R J, Klibanov S, Pina M L, Alber S M, Watkins S C, Brandenburger G H & Wagner W R 1998 *Circulation* **98**(1), 1.

Wickline S A, Hughes M, Ngo F C, Hall C S, Marsh J N, Brown P A, Allen J S, McLean M D, Scott M J & Fuhrhop R W 2002 *Academic Radiology* **9**(2), S290–S293.

Yamaguchi K & Anderson J M 1993 *Journal of Controlled Release* **24**(1-3), 81–93.

Yanagisawa K, Moriyasu F, Miyahara T, Yuki M & Iijima H 2007 *Ultrasound in medicine & biology* **33**(2), 318–325.

Ye Z 1996 *The Journal of the Acoustical Society of America* **100**, 2011.

Yeh C K & Su S Y 2008 *Ultrasound in Medicine and Biology* **34**(8), 1281–1291.

Zheng L J, Tu J & Chen W Z 2009 *Chinese Science Bulletin* **54**, 3501–3507.